

# CrystEngComm

Accepted Manuscript



This is an *Accepted Manuscript*, which has been through the Royal Society of Chemistry peer review process and has been accepted for publication.

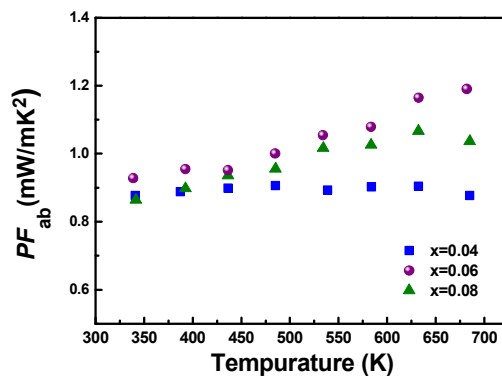
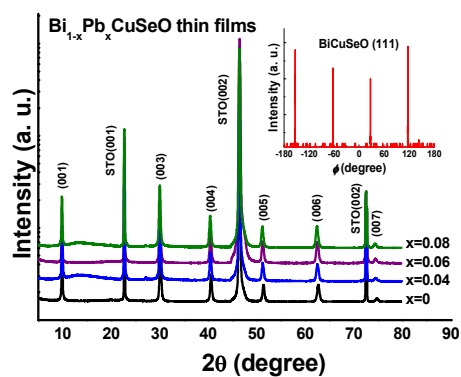
*Accepted Manuscripts* are published online shortly after acceptance, before technical editing, formatting and proof reading. Using this free service, authors can make their results available to the community, in citable form, before we publish the edited article. We will replace this *Accepted Manuscript* with the edited and formatted *Advance Article* as soon as it is available.

You can find more information about *Accepted Manuscripts* in the [Information for Authors](#).

Please note that technical editing may introduce minor changes to the text and/or graphics, which may alter content. The journal's standard [Terms & Conditions](#) and the [Ethical guidelines](#) still apply. In no event shall the Royal Society of Chemistry be held responsible for any errors or omissions in this *Accepted Manuscript* or any consequences arising from the use of any information it contains.

**A table of contents entry:**

Enhanced thermoelectric performance of *c*-axis oriented  $\text{Bi}_{1-x}\text{Pb}_x\text{CuSeO}$  single crystalline thin films



# Epitaxial growth and thermoelectric properties of *c*-axis oriented $\text{Bi}_{1-x}\text{Pb}_x\text{CuSeO}$ single crystalline thin films

Xiaolin Wu<sup>1</sup>, Jiang -Long Wang<sup>1</sup>, Hongrui Zhang<sup>2</sup>, Shufang Wang<sup>1,\*</sup>, Shengjun Zhai<sup>1</sup>,  
Yaguang Li<sup>1</sup>, Dogheche Elhadj<sup>3</sup> and Guangsheng Fu<sup>1,\*</sup>

<sup>1</sup> Hebei Key Lab of Optic-electronic Information and Materials, The College of Physics Science and Technology, Hebei University, Baoding 071002, China

<sup>2</sup> Beijing National Laboratory for Condensed Matter Physics, Institute of Physics, Chinese Academy of Sciences, Beijing 100190, China

<sup>3</sup> University of Valenciennes & Hainaut Cambrèsis, Institute of Electronic Microelectronic Nanotechnology IEMN CNRS, Le Mont Houy 59309 Valenciennes, France

E-mail: [sfwang@hbu.edu.cn](mailto:sfwang@hbu.edu.cn) and [fugs@hbu.edu.cn](mailto:fugs@hbu.edu.cn)

**Abstract:**

*c*-axis oriented  $\text{Bi}_{1-x}\text{Pb}_x\text{CuSeO}$  ( $0 \leq x \leq 0.8$ ) single crystalline thin films have been successfully epitaxially grown on  $\text{SrTiO}_3(001)$  substrates via pulsed laser deposition technique. Detailed x-ray diffraction and transmission electron microscopy measurements reveal the excellent *c*-axis and *ab*-plane texture of the films. As the Pb doping concentration increases, both the resistivity and Seebeck coefficient decrease due to the increase of hole carrier concentration. The highest power factor of about  $1.2 \text{ mWm}^{-1}\text{K}^{-2}$  has been achieved in  $\text{Bi}_{0.96}\text{Pb}_{0.06}\text{CuSeO}$  single crystalline thin films at 673 K, which is much higher than those of polycrystalline ceramics with random orientation, suggesting that *c*-axis oriented BiCuSeO-based single crystalline thin films might have great potential for application in thermoelectric thin film devices.

**Keywords:** BiCuSeO; single crystalline thin films; thermoelectric; *c*-axis oriented; epitaxial growth; pulsed laser deposition

## 1. Introduction

Thermoelectric (TE) materials, capable of converting thermal energy directly into electricity, making them attractive for waste heat conversion applications. The performance of TE materials is evaluated by the dimensionless figure of merit  $ZT=(S^2\sigma/\kappa)T$ , where  $S$ ,  $\sigma$ ,  $\kappa$  and  $T$  are the Seebeck coefficient, the electrical conductivity, the thermal conductivity and the absolute temperature, respectively. The state-of-the-art TE materials are primarily metallic alloys.<sup>1-4</sup> However, these materials often suffer from thermal instability at high temperatures, oxidation in air and toxicity. Oxides can overcome these problems and therefore have attracted increasing interests to the researchers. In the past decades, ZnO or In<sub>2</sub>O<sub>3</sub>-based transparent conductive oxides, SrTiO<sub>3</sub> or CaMnO<sub>3</sub>-based perovskite-type oxides, layered cobaltite etc. have been extensively studied as promising candidates for oxide TE materials.<sup>5-9</sup> However, their  $ZT$  values still remain significantly lower than those of metallic alloys.

BiCuSeO is a p-type oxide semiconductor with band gap of about 0.8 eV, which was previously studied as a potential transparent conducting material for photoelectric applications. It crystallizes in the ZrSiCuAs structure-type with a tetragonal P4/nmm layered structure. The lattice parameters of  $a$  and  $c$  are about 3.928 and 8.933 Å, respectively.<sup>10</sup> This structure is composed of insulating (Bi<sub>2</sub>O<sub>2</sub>)<sup>2+</sup> layers alternatively stacked with the conductive (Cu<sub>2</sub>Se<sub>2</sub>)<sup>2-</sup> layers along the  $c$ -axis. Recently, BiCuSeO was reported to exhibit potential TE applications due to its intrinsically low thermal conductivity.<sup>11,12</sup> Great efforts have been devoted to improve the TE performance of this compound via doping, copper vacancies, texture controlling, band tuning and

etc.<sup>13-24</sup> It was proved that *c*-axis textured BiCuSeO samples showed a significant enhancement in *ZT* relative to the randomly orientated ones due to its layered structure. A very high *ZT* of about 1.4 (~ 873 K), which actually is comparable to those reported for some state-of-art metallic alloys TE materials, has been obtained in the *c*-axis partial textured Ba-doped BiCuSeO polycrystalline ceramics,<sup>24</sup> and a greater *ZT* value can be expected to achieve if we can fabricate fully *c*-axis textured, i.e. *c*-axis oriented, samples.

For many microscale TE devices, thin films are highly required. In addition, thin films can offer tremendous scope for *ZT* enhancement via quantum confinement effect, interface engineering, nano-manipulation etc.<sup>25, 26</sup> Moreover, epitaxial thin films, with single crystalline structure, would also provide the possibility for a variety of very important experimental investigations and detailed anisotropy measurements on this material. However, so far there have been no reports on the TE properties of BiCuSeO-based *c*-axis oriented epitaxial thin films. In this paper, We report the epitaxial growth and TE properties of *c*-axis oriented Pb-doped BiCuSeO single crystalline thin films grown by pulsed laser deposition (PLD) technique. The resulting thin films show excellent crystalline quality as well as TE properties. A high power factor of about  $1.2 \text{ mWm}^{-1}\text{K}^{-2}$  has been achieved in  $\text{Bi}_{0.96}\text{Pb}_{0.06}\text{CuSeO}$  single crystalline thin films at 673 K, which is much higher than the values reported for the corresponding polycrystalline ceramics so far.<sup>13-15</sup>

## 2. Experimental section

$\text{Bi}_{1-x}\text{Pb}_x\text{CuSeO}$  ( $0 \leq x \leq 0.08$ ) single crystalline thin films were grown on (100) oriented

single crystal SrTiO<sub>3</sub> substrates by pulsed laser ablation of the corresponding ceramic targets under the atmosphere of high purity argon. Here the targets were synthesized by the solid-state reaction method as described follows: stoichiometric mixtures of Bi<sub>2</sub>O<sub>3</sub> (99.99%, Alfa Aesar), Cu (99.9%, Alfa Aesar), Bi (99.99%, Aladdin), Se (99.99%, Aladdin) and PbO (99.99 %, Alfa Aesar) powders were grinded for about 6 h by a ball-milling machine and pressed into pellets with diameter of about 30 mm. Then the pellets were sealed in quartz tubes under the pressure of 10<sup>-5</sup> Pa and sintered at 573 K for 6h and 973 K for 12h. Before loading into the PLD chamber, the SrTiO<sub>3</sub> substrates, having the cubic structure with lattice parameters of about 3.905 Å, were cleaned in an ultrasonic bath for 10 min in acetone, followed by isopropyl alcohol, de-ionized water and then spun dry. An excimer laser with 308 nm radiation was used for PLD with a laser energy density of 1.5 J/cm<sup>2</sup> and a repetition rate of 3 Hz. The distance between substrate and target was about 50 mm, and the argon pressure of 0.1 Pa was maintained during the film growth at the optimization substrate temperature of 350 °C. After the deposition, the films were cooled to room temperature within 20 min.

The thickness of the films was measured by the Step Profiler (Dektak 150) and all film samples used in this work was about 50 nm. The crystal structure of the films was measured using a Bruker AXS D8 advance x-ray diffractometer with *Cu Kα* radiation. The surface morphology of the films was analyzed by atomic force microscopy (AFM, Nanoscope IV, Digital Instruments) with a tapping mode. The microstructure and the elemental compositions of the films were analyzed with a

field-emission transmission electron microscopy (TEM, Tecnai G2 F20) equipped with an energy-dispersive X-ray spectroscopy (EDX) detector. The room temperature carrier concentration  $n$  and carrier mobility  $\mu$  were measured by using a physical properties measurement system (PPMS-9, Quantum Design Inc.) with the Van Der Pauw method. Electrical resistivity  $\rho$  and Seebeck coefficient  $S$  were measured simultaneously by the standard dc four-probe technique from 300 K to 673 K in a LSR-800 measurement system (Linseis, Germany).

### 3. Results and discussion

Figure 1a shows x-ray diffraction (XRD)  $\theta$ - $2\theta$  scans of  $\text{Bi}_{1-x}\text{Pb}_x\text{CuSeO}$  ( $0 \leq x \leq 0.08$ ) thin films on (001)  $\text{SrTiO}_3$  substrates. Apart from the substrate peaks, all diffraction peaks can be indexed by  $\text{BiCuSeO}$  (0 0  $l$ ) characteristic peaks (PDF# 45-0296), indicating the resulting films are pure phase and  $c$ -axis oriented. As Pb doping concentration  $x$  increases, the diffraction peaks systematically shift toward small angle, as seen in figure 1b, suggesting  $c$ -axis lattice parameters of the films increase due to the substitution of  $\text{Pb}^{2+}$  for  $\text{Bi}^{3+}$  (the ionic radius of Pb and Bi is about 1.29Å and 1.17Å in a coordination number of 8 as given by Shannon)<sup>27</sup>. The inset of figure 1b is the  $\omega$ -scan of (0 0 3) peak for the  $x=0$  thin film sample (i.e.  $\text{BiCuSeO}$ ), it shows a full width at half maximum (FWHM) of  $0.35^\circ$ , further confirming the excellent  $c$ -axis orientation of the film. Figure 1c presents the reciprocal space mapping (RSM) of the  $\text{BiCuSeO}$  thin film sample. It clearly reveals that the strain in this 50-nm-thick film is fully relaxed. Similar results are obtained for other  $\text{Bi}_{1-x}\text{Pb}_x\text{CuSeO}$  thin films with the same thickness. This result suggest that the lattice parameters shift shown in figure 1b

is indeed caused by the substitution of  $\text{Pb}^{2+}$  for  $\text{Bi}^{3+}$  but not by lattice strain or residual stresses. The *ab*-plane or *in*-plane texture information of the  $\text{Bi}_{1-x}\text{Pb}_x\text{CuSeO}$  films on  $\text{SrTiO}_3(001)$  was investigated by XRD  $\phi$  scan. Figure 1d presents the  $\phi$  scan of the (1 1 1) peak of the  $\text{BiCuSeO}$  film. It reveals the presence of four sharp peaks with FWHM of only about  $0.2^\circ$ , indicating the four-fold symmetry of the  $\text{BiCuSeO}$  film with a perfect *ab*-plane texture.

The *c*-axis oriented growth and good crystalline quality of the  $\text{Bi}_{1-x}\text{Pb}_x\text{CuSeO}$  thin films on  $\text{SrTiO}_3(001)$  were further investigated by TEM. Figure 2a presents a high-resolution TEM (HRTEM) picture of  $\text{BiCuSeO}$  thin film on  $\text{SrTiO}_3(001)$  substrate. Well-ordered layered structures of  $\text{BiCuSeO}$  stacked along the *c* axis can be clearly observed in the picture. In addition, there exists a bright area with 1-2 nm in width at the interface between the film and the substrate. This imperfect interface is suggested to be caused by the lattice mismatch between  $\text{BiCuSeO}$  and  $\text{SrTiO}_3$ . The enlarged HRTEM of the film part is illustrated in figure 2b, and the distance of the lattice in HRTEM, which is about 0.892 nm, is consistent with the *c* lattice parameter obtained from XRD. The corresponding selected area electron diffraction (SAED) pattern, shown in the figure 3c, confirms the epitaxial growth of  $\text{BiCuSeO}$  film on  $\text{SrTiO}_3$ , evidenced by the distinguished diffraction dots from the film and the substrate. The epitaxial relationship between the film and the substrate deduced from the SAED pattern is  $\text{BiCuSeO}[100]//\text{SrTiO}_3[100]$ . Figure 2e presents the AFM image of this  $\text{BiCuSeO}$  thin film. The film is dense and free of any microcracks or pores. Moreover, it exhibits a very smooth surface with root mean square (rms) roughness of

only 4.5 nm over the 10  $\mu\text{m}\times 10\ \mu\text{m}$  large scanning range.

Elemental analysis and chemical characterization of the film samples were studied using TEM-EDX. Figure 3a presents low-magnification cross-sectional scanning TEM (STEM) image of the 50-nm-thick BiCuSeO thin film on SrTiO<sub>3</sub>. The EDX analysis of the film, as seen in figure. 3b, reveals that the cation ion ratio of Bi:Cu:Se in the film is about 1.00:1.06:1.03, which is very close to that of the nominal composition of this material. We also performed the EDX measurement on a large scale of SEM surface image of the present film, and similar results were obtained. Figure 3c-e illustrate the EDX mapping of Bi, Cu, and Se elements of the film, demonstrating the homogeneous distribution of these elements in the film, and no obvious elemental diffusion between the film and substrate near the interface.

Figure 4a and 4b present the temperature dependence of the *ab*-plane resistivity  $\rho_{ab}$  as well as Seebeck coefficient  $S_{ab}$  of Bi<sub>1-x</sub>Pb<sub>x</sub>CuSeO thin films with x=0.04, 0.06 and 0.08, respectively. It shows that the resistivity of all doped films increases with temperature over the whole temperature range, suggesting a metallic-like conducting behavior. With the increase of Pb doping concentration x, the resistivity of the films decreases due to the increased hole carrier concentration induced by the substitution of Pb<sup>2+</sup> for Bi<sup>3+</sup>. Moreover, the resistivity of all films is smaller than that of corresponding polycrystalline ceramics, which is mainly caused by the *c*-axis orientated feature of the films. It has been known that the electrical transport in the BiCuSeO system is anisotropic and the resistivity in the *ab*-plane is much lower than that along *c*-axis direction.<sup>24</sup> The Seebeck coefficient of all films shown in figure 4b is

positive, indicating the major carriers are holes. As the Pb doping concentration  $x$  increases, the hole carrier concentration in the  $\text{Bi}_{1-x}\text{Pb}_x\text{CuSeO}$  films increases and thus the corresponding Seebeck coefficient decreases. We calculated the  $ab$ -plane power factor  $PF_{ab}$  ( $PF_{ab}=S_{ab}^2/\rho_{ab}$ ) of all films at different temperatures according to the corresponding  $\rho_{ab}$ - $T$  and  $S_{ab}$ - $T$  data, which is shown in figure 4c. The film with  $x=0.06$  shows the best power factor. Moreover, all film samples exhibit greatly enhanced power factors as compared to those reported for the corresponding polycrystalline ceramics in literatures because of their low resistivity induced by the perfect  $c$ -axis oriented growth.<sup>13-15</sup> For example, the power factor of  $\text{Bi}_{0.94}\text{Pb}_{0.06}\text{CuSeO}$   $c$ -axis oriented film is about  $1.2 \text{ mWm}^{-1}\text{K}^{-2}$  at 673 K, which is about 1.5 times larger than the best value so far obtained from the polycrystalline ceramics with random orientation.<sup>15</sup> It needs to be mentioned here that we have not provided the  $\rho_{ab}$ - $T$  and  $S_{ab}$ - $T$  data for  $x=0$  sample (i. e.  $\text{BiCuSeO}$  thin film) because the resistance of this sample is too large at higher temperatures and beyond the maximum measurement limit of the LSR-800 system. The room temperature  $\rho_{ab}$  and  $S_{ab}$  of the  $x=0$  film sample are measured to be  $12.5 \text{ m}\Omega \text{ cm}$  and  $202 \text{ }\mu\text{V/K}$  respectively, and the calculated power factor  $PF_{ab}$  is about  $0.33 \text{ mWm}^{-1}\text{K}^{-2}$ . This power factor is much lower than that of the Pb-doped film samples shown in figure 4c, confirming that Pb-doping can improve the TE performance of  $\text{BiCuSeO}$  thin films.

Although we have not yet obtained the  $ab$ -plane thermal conductivity  $\kappa_{ab}$  of the present  $\text{Bi}_{1-x}\text{Pb}_x\text{CuSeO}$   $c$ -axis oriented thin films due to the difficulty in measuring  $\kappa_{ab}$  for thin film samples, we can expect that the films have a much reduced thermal

conductivity due to their small crystallite sizes (about 50 nm) as well as the enhanced phonon scatterings at film surface and film/substrate interface.<sup>28-31</sup> For example, the measured  $\kappa_{ab}$  of a 50 nm-thick crystalline Si film was reported to be only about 1/3 of the bulk value at room temperature.<sup>29</sup> Therefore, higher  $ZT$  values than those of polycrystalline ceramics can be achieved in the present  $\text{Bi}_{1-x}\text{Pb}_x\text{CuSeO}$   $c$ -axis oriented films.

#### 4. Conclusion

In conclusion,  $c$ -axis oriented  $\text{Bi}_{1-x}\text{Pb}_x\text{CuSeO}$  ( $0 \leq x \leq 0.08$ ) single crystalline thin films have been successfully epitaxially grown on (001)  $\text{SrTiO}_3$  substrates. The resulting films exhibit single-crystal-like structures with perfect texture both in  $ab$ -plane and along  $c$ -axis. As the Pb doping concentration increases, both the resistivity and Seebeck coefficient of the films decrease due to the increased hole carrier concentration. Moreover, due to the good  $c$ -axis oriented feature of the films, all films exhibited a reduced electrical resistivity in comparison to that of the corresponding polycrystalline ceramics, leading to an enhanced power factor. The highest power factor of about  $1.2 \text{ mWm}^{-1}\text{K}^{-2}$  was achieved in  $\text{Bi}_{0.96}\text{Pb}_{0.06}\text{CuSeO}$  single crystalline thin films at about 673 K, which is much higher than those reported for polycrystalline ceramics with random orientation. The high quality crystalline structure, smooth surface as well as good TE performance of these  $c$ -axis oriented  $\text{BiCuSeO}$ -based single crystalline thin films pave the way for their potential applications in TE thin film devices.

## Acknowledgments

This project was supported by the National Natural Science Foundation of China (No. 51372064), the Nature Science Foundation of Hebei Province, China (No. 2013201249 and No. A2014201176).

## References

1. G. J. Snyder, E. S. Toberer, *Nat. Mater.*, 2008, **7**, 105-114.
2. B. Poudel, Q. Hao, Y. Ma, Y. C. Lan, A. Minnich, B. Yu, X. Yan, D. Z. Wang, A. Muto, D. Vashaee, X. Y. Chen, J. M. Liu, M. S. Dresselhaus, G. Chen, Z. F. Ren, *Science*, 2008, **320**, 634-638.
3. H. Y. Fang, Z. Q. Luo, H. R. Yang, Y. Wu, *Nano Lett.*, 2014, **14**, 1153-1157.
4. Z. L. Sun, S. C. Liufu, X. H. Chen, L. D. Chen, *ACS Appl. Mater. Interfaces*, 2011, **3**, 1390-1393.
5. N. V. Nong, N. Pryds, S. Linderoth, M. Ohtaki, *Adv. Mater.*, 2011, **23**, 2484-2490.
6. X.B. Zhu, X.W. Tang, D.Q. Shi, H.B. Jian, H.C. Lei, W.K. Yeoh, B.C. Zhao, J. Yang, Q. Li, R.K. Zheng, S.X. Dou, Y.P. Sun, *Dalton Trans.* 2011, **40**, 9544-9550
7. M. Lee, L. Viciu, L. Li, Y.Y. Wang, M.L. Foo, S. Watauchi, R.A. Pascal jr, R.J. Cava, N. P. Ong, *Nature Mater.*, 2006, **5**, 537-540.
8. J. -L. Lan, Y. C. Liu, Y. -H. Lin, C. -W. Nan, Q. Cai, X. P. Yang, *Scientific Reports*, 2015, **5** , 7783.
9. P. Jood, R. J. Mehta, Y. L. Zhang, G. Peleckis, X. L. Wang, R. W. Siegel, T.

- Borca-Tasciuc, S. X. Dou, G. Ramanath, *Nano Lett.*, 2011, **11**, 4337-4342.
10. C. Barreteau, D. Berardan, E. Amzallag, L. -D. Zhao, N. Dragoe, *Chem. Mater.*, 2012, **24**, 3168-3178
11. L. -D. Zhao, D. Berardan, Y. L. Pei, C. Byl, L. Pinsard-Gaudart, N. Dragoe, *App. Phy. Lett.*, 2010, **97**, 092118.
12. L. -D. Zhao, J. Q. He, D. Bérardan, Y. -H. Lin, J. -F. Li, C. -W. Nan, N. Dragoe, *Energy Environ. Sci.*, 2014, **7**, 2900-2924.
13. L. Pan, D. Bérardan, L. -D. Zhao, C. Barreteau, N. Dragoe, *App. Phy. Lett.*, 2013, **102**, 023902.
14. S. D. N. Luu, P. Vaqueiro, *J. Mater. Chem. A*, 2013, **1**, 12270-12275.
15. Y. -C. Liu, J. -L. Lan, B. Zhan, J. X. Ding, Y. Liu, Y. -H. Lin, B. P. Zhang, C. -W. Nan, *J. Am. Ceram. Soc.*, 2013, **96**, 2710-2713.
16. J. -L. Lan, Y. -C. Liu, B. Zhan, Y. -H. Lin, B. P. Zhang, X. Yuan, W. Q. Zhang, W. Xu, C. -W. Nan, *Adv. Mater.*, 2013, **25**, 5086-5090.
17. J. Li, J. H. Sui, Y. L. Pei, C. Barreteau, D. Bérardan, N. Dragoe, W. Cai, J. Q. He, L. -D. Zhao, *Energy Environ. Sci.*, 2012, **5**, 8543-8547.
18. Y. -L. Pei, H. J. Wu, D. Wu, F. S. Zheng, J. Q. He, *J. Am. Chem. Soc.*, 2014, **136**, 13902-13908
19. C. Barreteau, D. Bérardan, L. -D. Zhao, N. Dragoea, *J. Mater. Chem. A*, 2013, **1**, 2921-2926.
20. Y. -L. Pei, J. Q. He, J. -F. Li, F. Li, Q. J. Liu, W. Pan, C. Barreteau, D. Bérardan, N. Dragoe, L. -D. Zhao, *NPG Asia Materials*, 2013, **5**, e47.

21. Y. Liu, J. L. Lan, W. Xu, Y. C. Liu, Y. -L. Pei, B. Cheng, D. -B. Liu, Y. -H. Lin, L. -D. Zhao, *Chem. Commun.*, 2013, **49**, 8075-8077.
22. W. Xu, Y. Liu, L. -D. Zhao, P. F. An, Y. -H. Lin, A. Marcellie, Z. Y. Wu, *J. Mater. Chem. A*, 2013, **1**, 12154-12158.
23. Y. Liu, L. -D. Zhao, Y. C. Liu, J. L. Lan, W. Xu, F. Li, B. P. Zhang, D. Berardan, N. Dragoe, Y. -H. Lin, C -W. Nan, J. -F. Li, H. M. Zhu, *J. Am. Chem. Soc.* 2011, **133**, 20112–20115.
24. J. H. Sui, J. Li, J. Q. He, Y. L. Pei, D. Berardan, H. J. Wu, N. Dragoe, W. Cai, L. -D. Zhao, *Energy Environ. Sci.*, 2013, **6**, 2916–2920.
25. R. Venkatasubramanian, E. Siivola, T. Colpitts, B. O'Quinn, *Nature*, 2001, **413**, 597-602.
26. H. Ohta, S. W. Kim, Y. Mune, T. Mizoguchi, K. Nomura, S. Ohta, T. Nomura, Y. Nakanishi, Y. Ikuhara, M. Hirano, H. Hosono, K. Koumoto, *Nat. Mater.*, 2007, **6**, 129-134.
27. R. D. Shannon, *Acta Cryst.* 1976, **A32**, 751
28. A. J. H. McGaughey, E. S. Landry, D. P. Sellan, C. H. Amon, *Appl. Phys. Lett.*, **2011**, **99**, 131904.
29. Y. S. Ju, *Appl. Phys. Lett.*, 2005, **87**, 153106.
30. Y. F. Hu, E. Sutter, W. D. Si, Q. Li, *Appl. Phys. Lett.*, 2005, **87**, 171912.
31. Y. Sun, M. Christensen, S. Johnsen, N. V. Nong, Y. Ma, M. Sillassen, E. Y. Zhang, A. E. C. Palmqvist, J. Bøttiger, B. B. Iversen, *Adv. Mater.*, 2012, **24**, 1693–1696.

**Figure captions:**

Figure 1. XRD patterns for  $\text{Bi}_{1-x}\text{Pb}_x\text{CuSeO}$  ( $0 \leq x \leq 0.8$ ) thin films on (001)  $\text{SrTiO}_3$  substrate. (a)  $\theta$ - $2\theta$  scans; (b) the magnified curves of  $\text{Bi}_{1-x}\text{Pb}_x\text{CuSeO}$  (003) peak. The inset is the  $\omega$ -scan of the (003) peak; (c) the reciprocal space mapping of the 50-nm-thick  $\text{BiCuSeO}$  thin film sample; (d)  $\phi$  scan of the (111) peak for the  $\text{BiCuSeO}$  thin film sample.

Figure 2. (a) HRTEM cross-sectional image of a  $\text{BiCuSeO}$  thin film on (001)  $\text{SrTiO}_3$  substrate; (b) the magnified HRTEM image of the film part; (c) the corresponding SEAD pattern of the  $\text{BiCuSeO}/\text{SrTiO}_3$  cross section; (d) AFM image of the  $\text{BiCuSeO}$  thin film over a scanning area of  $10 \times 10 \mu\text{m}$ . The electron beam incident direction in Fig. 2(a)-(c) is all along the [001] direction.

Figure 3. (a) Low-magnification cross-sectional STEM image of a 50-nm-thick  $\text{BiCuSeO}$  thin film on (001)  $\text{SrTiO}_3$  substrate; (b) EDX spectroscopy derived from the film; (d-e) EDX mapping of Bi, Cu and Se elements of the film.

Figure 4. The temperature dependence  $ab$ -plane (a) resistivity  $\rho_{ab}$ ; (b) Seebeck coefficient  $S_{ab}$ ; (c) power factor  $PF_{ab}$  of the  $\text{Bi}_{1-x}\text{Pb}_x\text{CuSeO}$  ( $x=0.04, 0.06$  and  $0.08$ ) thin films on (001)  $\text{SrTiO}_3$ .

Figure 1

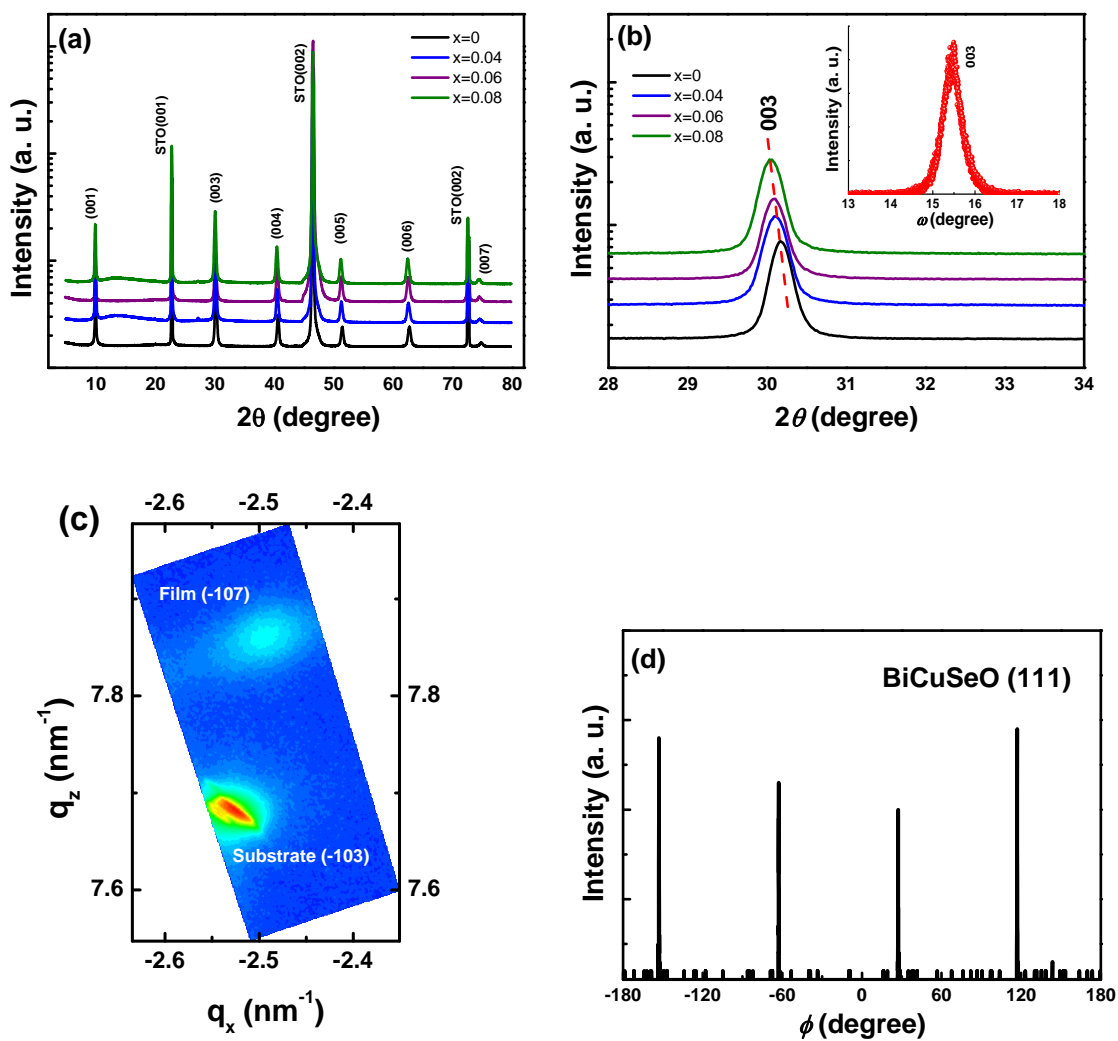


Figure 2

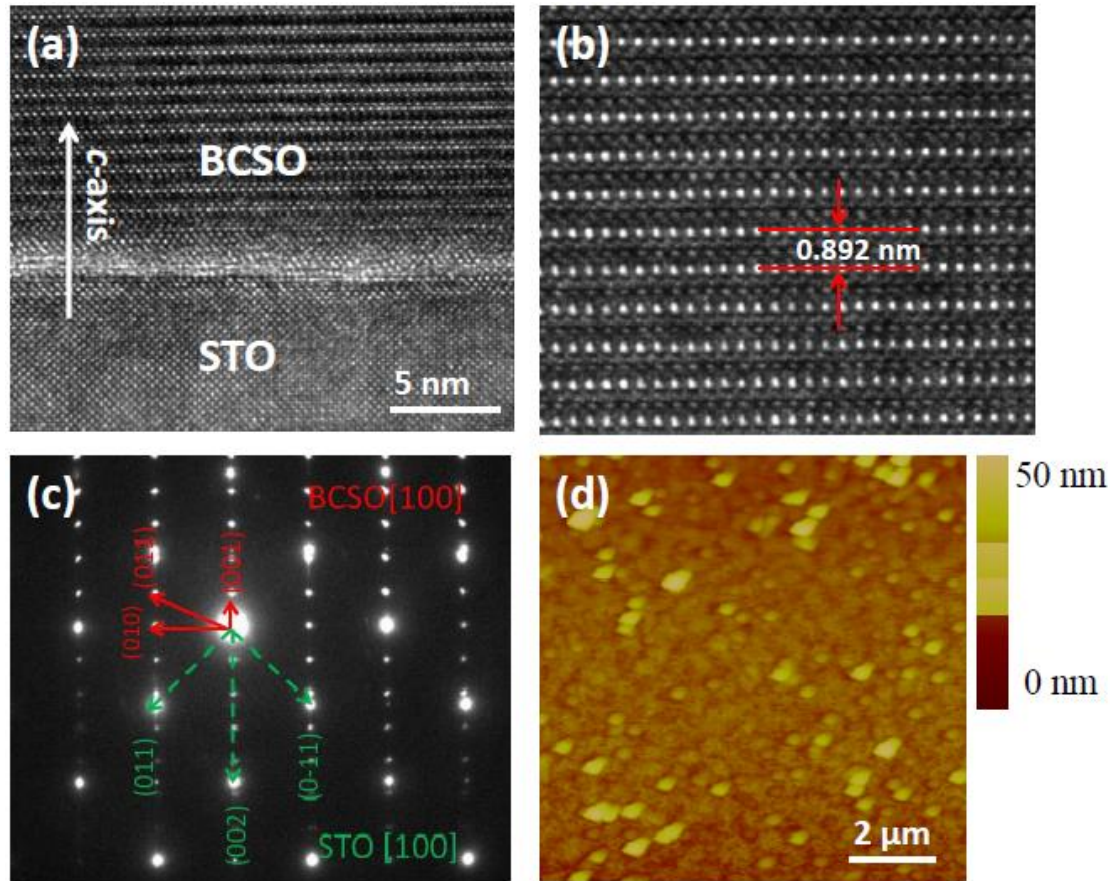


Figure 3

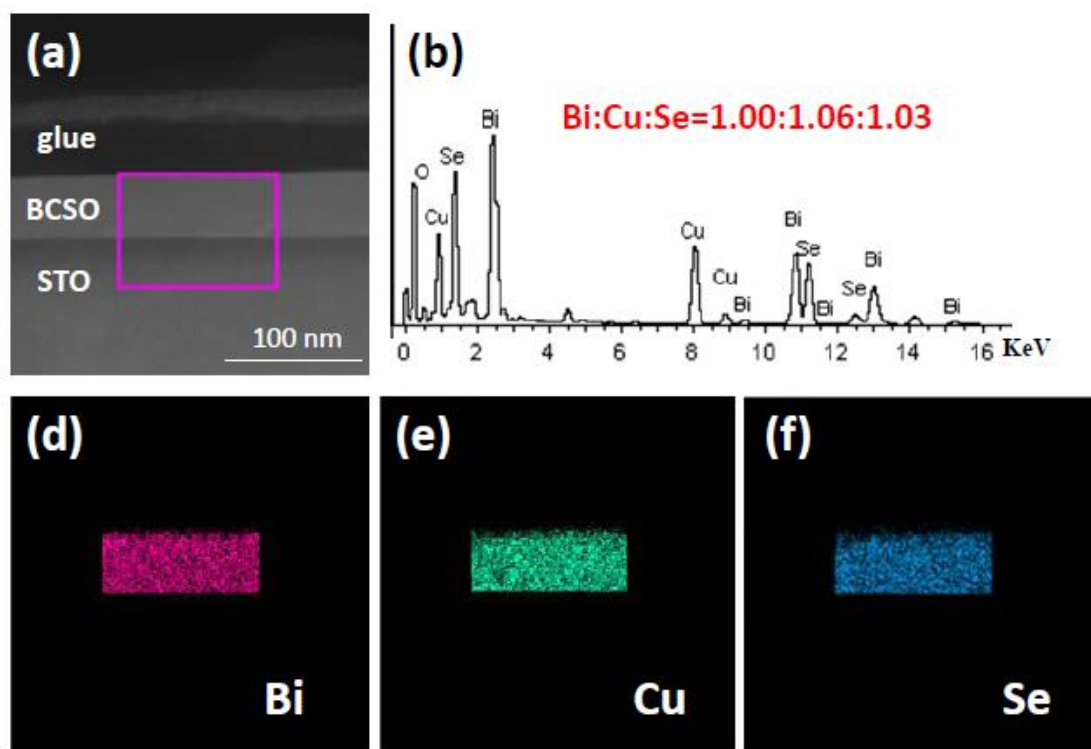


Figure 4

